Electronic properties of $PbMo_6S_8$ and $Cu_xMo_6S_8$

John A. Woollam and Samuel A. Alterovitz*
NASA Lewis Research Center, Cleveland, Ohio 44135
(Received 26 June 1978)

Normal-state properties of sputtered, evaporated, and sintered $PbMo_6S_8$ and $Cu_xMo_6S_8$ samples are reported ($1.6 \leq x \leq 2.5$). These include the temperature dependence of resistivity, magnetoresistance, and Hall effect. When combined with superconducting properties (measured on the same samples) and theory, a number of Fermi-surface and superconducting parameters are derived. Fits to the temperature dependence of the resistivity are compared with similar fits for A-15 structure superconductors.

I. INTRODUCTION

The superconducting ternary molybdenum sulfides (TMS) have been of recent interest because of their record-high critical fields[1,2] B_{c2}, moderately high superconducting transition temperatures[1,2] T_c, and potential for carrying high currents at high magnetic fields.[3] They were first synthesized by Chevrel,[4,5] are sometimes called Chevrel-phase materials, and have the rhombohedral structure shown in Fig. 1 for $PbMo_6S_8$. The general chemical formula is $M_xMo_6S_8$, where M is any of many possible metals, and x depends on the particular compound. Some TMS have been formed with rare-earth metals as one element of the ternary structure, and this results in interesting magnetic properties.[6]

Heat-capacity and neutron scattering experiments have been done, and they reveal unusual phonon spectra.[7-9] As with other high T_c superconductors, the TMS exhibit phonon softening and lattice instabilities as temperatures are lowered.[10]

$PbMo_6S_8$ exhibits a relatively narrow region of ternary phase stability with respect to Pb concentration.[11] Contrary to this, the $Cu_xMo_6S_8$ system[12] can be formed over the range $1.5 \leq x \leq 3.6$. Figure 2 shows the equilibrium phase diagram as reported by Flükiger *et al.* from measurements on single-crystal samples prepared by melting under argon pressure.[12] It shows two low-temperature variations of the ternary structure, LT1 and LT2. No x-ray data are as yet available for the low-temperature phases. (Boundaries were determined by heat-capacity, resistivity, and magnetic susceptibility anomalies.) The T_c's for LT1 and LT2 are near 11 and 6 K, respectively. Because of structural phase changes, the electronic properties of $Cu_xMo_6S_8$ exhibit structure as temperature is varied below room temperature.

For the $PbMo_6S_8$ system there was no structure in the resistance versus temperature data from T_c to well above 300 K and results over this temperature range could be compared with theories for resistivity in d-band metals. For $Cu_xMo_6S_8$ data are compared to theory for temperatures below the phase transitions. Results on both materials were strikingly similar to results on A-15 materials. Thus models for A-15 behavior are applied to TMS for comparison. This is not an unreasonable procedure since both A-15's and TMS's are high-temperature superconductors[13,14] having moderate to strong electron-phonon coupling and a high density of states at the Fermi energy. Both materials exhibit an apparent T^2 behavior in resistivity at low T, an inflection point at intermediate temperature, and a tendency towards saturation at high temperature.[15-17] Thus, we now briefly review the models proposed to explain resistivity data in A-15 superconductors.

Woodard and Cody[18] described data on Nb_3Sn by an empirical fit to

$$\rho(T) = \rho_0 + bT + de^{-T_0/T}, \tag{1}$$

where ρ_0 is the residual resistivity, and b, d, and T_0 are constants. Data fit to better than 1% over 18 K $\leq T \leq$ 850 K with $T_0 = 85$ K. The explanation for the exponential was a possible phonon-assisted interband scattering from a low-mass s band to a high-mass d band. The exponential was then just a Boltzmann factor for the number of phonons available.

Cohen, Cody, and Halloran[19] introduced the "RCA model", which proposes a step function in the density of states near the Fermi energy E_F. The temperature dependence comes from s-d scattering and predicts a low-temperature T^3 term. Marchenko[20] found that data on V_3Si could be fit to

$$\rho = \rho_0 + bT^2 \tag{2}$$

for temperatures up to 29 K. Williamson *et al.*[21,22] found that

$$\rho = \rho_0 + b_nT^n + d_ne^{-T_0/T} \tag{3}$$

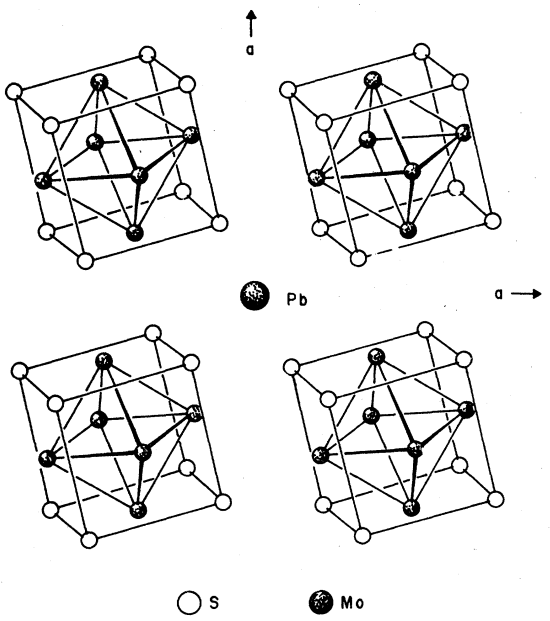

FIG. 1. Projection along (001) of a structure of $PbMo_6S_8$ (after Ref. 5).

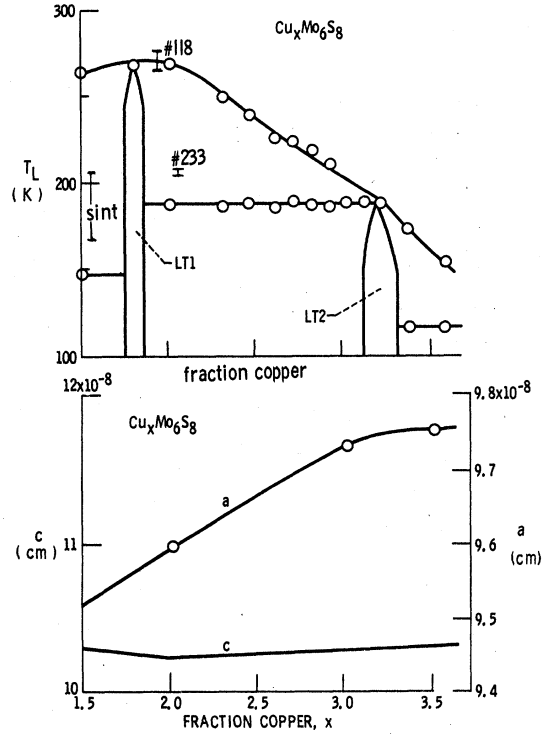

FIG. 2. Phase diagram (after Ref. 12) and lattice parameters (after Ref. 5) for $Cu_xMo_6S_8$, showing positions in temperature and x for structure in $R(T)$ vs T data for this work. Symbol "sint" is sintered $Cu_{1.6}Mo_6S_8$, a and c are rhombohedral lattice constants.

fit their Nb_3Sn, Nb_3Sb, and V_3Si data, where $n = 1$, $\frac{3}{2}$, or 2. T_0 was nearly independent of n, and the exponential was attributed to phonon-assisted interband scattering. They attribute the T^n term to intraband electron-electron scattering.

Bader and Fradin[23] used a model similar to the Cohen, Cody, and Halloran model, but used a Gaussian edge step in the density of states, and a generalized s-d scattering model. At low temperatures the non-Debye-like phonon spectra is responsible for the unusual T^2 behavior and at high temperature the density-of-states structure causes the resistivity to saturate.

The high-temperature saturation phenomena has also been called "deviation from linearity" (DFL), and has received much attention recently, especially for A-15 structure materials. In Bloch-Grüneisen theory the resistivity should be linear at high T. Mechanisms for DFL have been presented above. In addition, Allen *et al.*[24] suggest anharmonicity, but others[23] argue that this is too small to cause the observed DFL. Fisk and Webb[15] and others suggested that the DFL was due to the electron mean free path becoming comparable to the lattice spacing, and thus becomes "saturated" at high temperatures. This was supported by Allen,[25] but criticized by Laubitz *et al.*[26] Wiesmann *et al.*[27] proposed the empirical equation

$$\rho(T) = (\rho_0 + \rho_1 T)\{1 + [(\rho_0 + \rho_1 T)/\rho_{\max}]\}^{-1}, \qquad (4)$$

where $\rho_1 T$ is the first term in a series expansion. At high T, $\rho(T) \to \rho_{\max}$.

In this paper we present evidence for resistivity behavior in the TMS similar to that in the A-15's.[17] Our data are very nicely fit by Eq. (3) over most of the region from T_c to 300 K. At low T we find $\rho \sim T^2$ (or to T in the case of sintered $PbMo_6S_8$ for $14 \leq T \leq 40$ K). At high temperatures we can fit the data reasonably well to Eq. (4), and this gives a value for $\rho_{\max}$. This is used along with Hall-effect data[28] and superconductivity data on the same samples to get values for the effective mass, the Fermi velocity, the BCS coherence length, and Fermi-surface area ratios.[29] Magnetoresistance measurements give values of electron mobilities. Coherence length to mean-free-path ratios indicate that our TMS are intermediate between clean and dirty superconductor limits.

II. EXPERIMENTAL METHODS

Samples were prepared by sintering,[30] sputtering,[31] and by coevaporation.[32-35] For the $Cu_xMo_6S_8$ samples the x values were determined from x-ray lattice parameter measurements and data from Chevrel's thesis (Fig. 2). An electron microprobe was also used to determine whether the

distribution of various elements in the sample were uniform. A scanning electron microscope and transmission electron microscope photos were also taken to examine sample morphology. All but the sintered samples were prepared on heated sapphire substrates.

Resistance versus temperature data were taken using a conventional four-probe technique, using either ac or dc currents. For ac currents a lock-in amplifier was used for detection and signal to noise was approximately 10^5. The dc data has a much lower signal-to-noise ratio ($\sim 10^3$), and was used as a check on the overall features of the ac data. Temperatures were measured with carbon and carbon glass thermometers, as well as with gallium arsenide diode thermometers. Relative temperatures were accurate to within ± 0.1 K at low temperatures and to within ± 0.8 K near room temperature.

For magnetoresistance measurements dc currents were used and data were taken in two ways. In the first method the temperature was established at zero field using a carbon thermometer. Constant temperature was maintained while the magnetic field was changed, using a glass ceramic thermometer in an ac bridge temperature-control circuit. The second method was to sweep the temperature over several degrees while at a series of fixed magnetic fields. The magnetoresistance of the carbon thermometer was measured independently, and corrections made to temperature readings. The second method was preferred since it was somewhat more accurate and because it displayed trends of magnetoresistance with temperature.

Samples and thermometers were mounted on a platform inside a double-chamber probe. The inner chamber containing the sample and thermometers was filled with helium exchange gas and the outer region was under vacuum. The outside of the inner can was wound with a wire heater to control temperature, and the entire probe was immersed in either liquid helium or liquid nitrogen. For magnetoresistance measurements a 14 T superconducting solenoid was used, having a liquid-helium insert Dewar. Fields were measured with calibrated magnetoresistors. For the Hall-effect measurement[28] samples were immersed directly in liquid nitrogen and pumped liquid nitrogen to maintain temperature stability. Field and current reversals were made for these measurements using a 7-T water-cooled magnet.

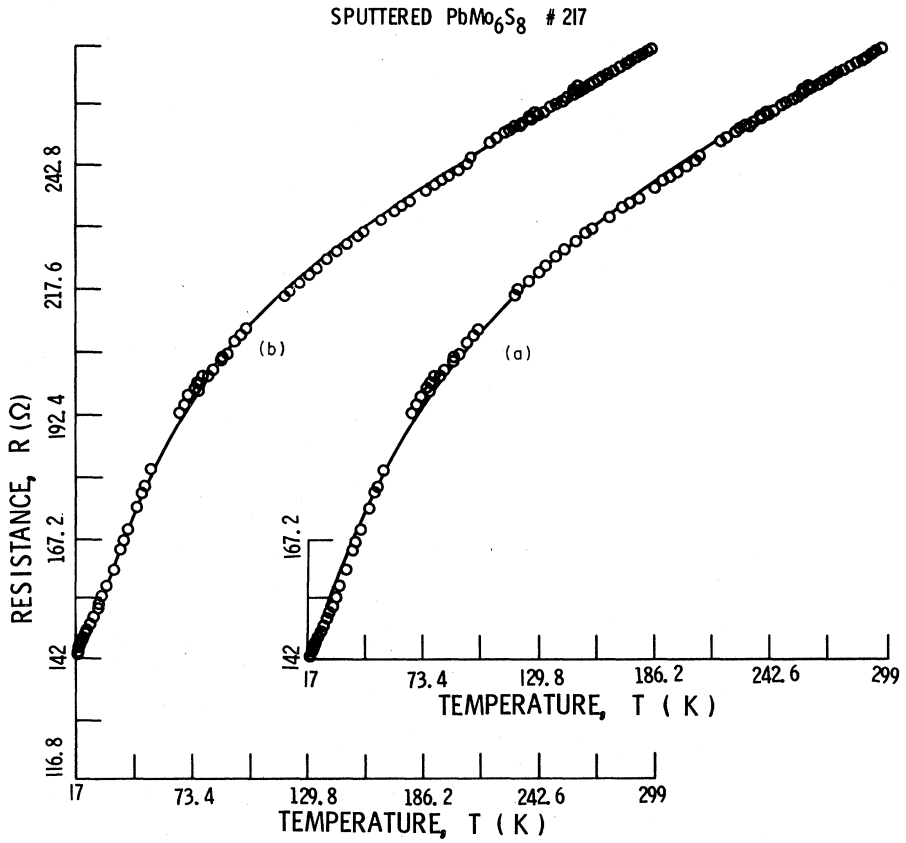

FIG. 3. Resistance vs temperature plots for sputtered $PbMo_6S_8$ (No. 217). Solid curve is a least-squares fit from Eq. (3) with (a) $d_n = 0$, $n = 0.2$ and (b) $n = 2.34$.

TABLE I. Summary of least-squares fits to Eqs. (3) and (4) over wide temperature ranges, as well as superconducting and galvanomagnetic properties.

		Eq. (3)					Eq. (4)		Superconducting slope transition T_c		Eq. (5)		Resistance and Hall data	
Sample	Range of fit	T_0 (K)	n	R [a]	T_{infl}	Root-mean-square deviation of data from best fit (%)	ρ_{max}/ρ_0	l^c (Å)	T_c (K)	$-(dH_{c2}/dT)_{T_c}$ (T/K)	Mobility $\bar{\mu}$ (cm^2/V sec)	ρ_{300K}/ρ_0	R_H (esu)	Carrier density (holes)
Sputtered	17–300 K	50.1	1	2	25	0.5	3.6	23	11.5	5.5–6.0	80	2	0.9×10^{-24}	$0.7 \times 10^{23}/cm^3$
$PbMo_6S_8$		57	2	7	···	0.4								
No. 217		59.3	2.34	10	30	0.4								
		b	0.2	b	···	0.9								
Evaporated	11–220 K	78.4	1	0.9	39	0.2	5	32	10.8	2.08	27	2.8	$\leq \lvert 1.6 \rvert \times 10^{-24} \geq 0.4 \times 10^{23}/cm^3$	
$Cu_{2.5}Mo_6S_8$		76.4	2	2.8	···	0.5								
No. 39		79.9	0.96	0.8	39	0.3								
		b	0.67	b	···	1.8								
Sputtered	11–220 K	92.5	1	1.4	46	0.6	7	46	10.3	2.25	not	4.8	not	···
$Cu_2Mo_6S_8$		91.0	2	4.1	···	1.0					measured		measured	
No. 118		111.7	1.64	0.8	56	0.6								
		b	0.62	b	···	3.2								
Sputtered	13–157 K	105	1	0.6	53	0.2	<7	46	9.8	2.0	42	2.8	$+2.3 \times 10^{-24}$	$0.3 \times 10^{23}/cm^3$
$Cu_2Mo_6S_8$		81.1	2	1.2	···	0.2								
No. 233		84.6	1.38	0.8	47	0.1								
		b	0.98	b	···	1.2								
Sintered	12–92 K	115	1	0.4	58	0.8	30	200	10.5	1.85	300	5.3	not	···
$Cu_{1.6}Mo_6S_8$		64.1	2	0.3	···	0.6							measured	
		67	1.56	0.3	···	0.6								
		b	1.2	b	···	1.1								
Sintered	18–300 K	85	1.0	0.64	d	0.5	3.5	23	14	···	37	2.6	not	···
$PbMo_6S_8$		90	2.0	0.32	d	0.7							measured	
No. 1		b	0.24	b	d	0.17								

[a] Ratio of third to second term in Eq. (3) evaluated at 200 K.
[b] Fits made to Eq. (3) with $d_n = 0$; therefore, T_0 and R have no meaning.
[c] Assumes saturated ρ_{max} when $l = 6.5$ Å. In the Table l is the mean free path at low temperatures.
[d] Inflection near or below lowest data point at 18 K.
[e] Fits to Eq. (3) for sintered $PbMo_6S_8$ (No. 1 are not too meaningful—see text).

III. EXPERIMENTAL RESULTS

A. Power-law and exponential fits to resistance versus temperature data

Attempts were made to fit data for the temperature region from T_c to 300 K using Eq. (3) for the following samples: sputtered $PbMo_6S_8$ (No. 217), sintered $PbMo_6S_8$ (No. 1), evaporated $Cu_{2.5}Mo_6S_8$ (No. 39), sputtered $Cu_2Mo_6S_8$ (No. 118), and sputtered $Cu_{2.1}Mo_6S_8$ (No. 233). Our data are presented as resistance R versus temperature rather than resistivity because of uncertainties of cross-sectional areas. Just above the superconducting transition resistivities are on the order of 100 $\mu\Omega$ cm. Equations (1)–(4) apply for either resistance or resistivity.

Four different least-squares fits were tried: (i) $n=1$, (ii) $n=2$, (iii) n used as a parameter in the fit, and (iv) n used as a parameter, but $d_n=0$. Examples of the types of fits are shown in Fig. 3 for sputtered $PbMo_6S_8$ (number 217). Poor fits are found for $d_n=0$ [Fig. 3(a)]. The best value of n determined by a least-squares fit, allowing ρ_0, b_n, n, d_n, and T_0 to be parameters, was $n=2.34$ [Fig. 3(b)]. However, the data are fit nearly as well if $n=2$. Parameters of the fits to the data are given in Table I, as are the root-mean-square deviations of data from the best fits. For the four fits to the $PbMo_6S_8$ (No. 217) data the value of T_0 ranged from 50 to 59 K. The $n=2.34$ and $n=2$ fits gave $T_0=59$ and 57 K, respectively. For $n=2$ and $n=2.34$ the exponential term dominates, being about a factor of 10 larger than the T^n term for this sample in the region near 200 K. At high T the T^n term becomes more important, but is still roughly a factor of 4–5 times smaller than the exponential term at 300 K. Williamson and Milewitz found similar behavior in Nb_3Sn, Nb_3Sb, and V_3Si: T_0 ranged from 85 K for Nb_3Sn to 210 K for Nb_3Sb, and the exponential term dominated over the T_n term.

Parameters in the fits for sintered $PbMo_6S_8$ data are shown in Table I. This material is very unusual in that ρ is proportional to T in the region from T_c to 40 K. Fits to Eq. (3) force the inflection in $\rho(T)$ to be near or below T_c and constants for such fits are given in Table I. Without an inflection in the experimental data for $\rho(T)$, constants for this sample are not too meaningful.

For the $Cu_xMo_6S_8$ samples, fits were made only over the temperature range up to 220 K, due to structure at phase transitions at higher T. In Fig. 4 plots similar to Fig. 3 are made for evaporated $Cu_{2.5}Mo_6S_8$ (No. 39). Again, fits are made for the cases $n=1$, $n=2$, n a parameter and $d_n=0$, and the latter two are shown in Fig. 4. Again, a very poor fit is found for $d_n=0$ [Fig. 4(a)], with the best fit giving $n=0.96$ [Fig. 4(b)]. The fits are not too sensitive to n over this (wide) temperature range, as is seen by the low root-mean-square deviation (Table I), indicating a reasonably good fit with $n=2$. In contrast to the $PbMo_6S_8$ case, the T^n term and the exponential terms are comparable for the range T_c to 200 K for all the $Cu_xMo_6S_8$. For $Cu_{2.5}Mo_6S_8$ (No. 39), T_0 is between 76 and 79 K. Again the T^n term be-

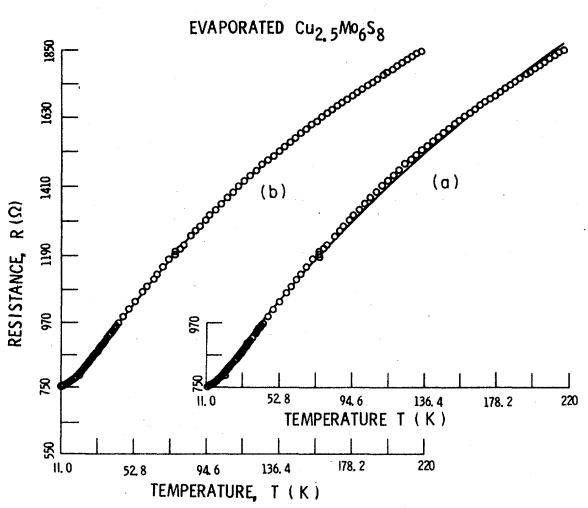

FIG. 4. Resistance vs temperature plots for evaporated $Cu_{2.5}Mo_6S_8$ (No. 39). Solid curve is a least-squares fit from Eq. (3) with (a) $d_n=0$, $n=0.67$, and (b) $n=0.97$.

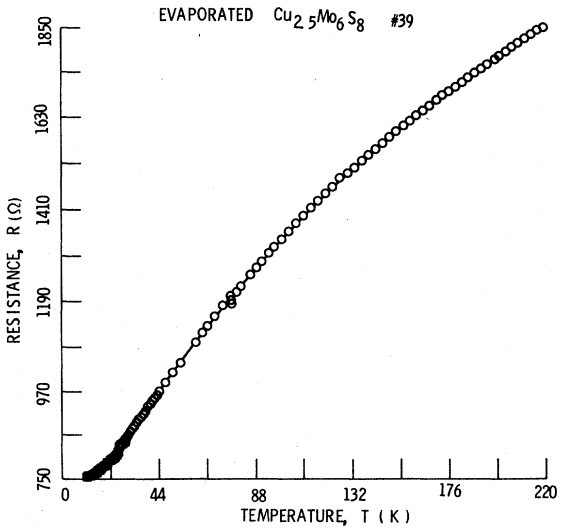

FIG. 5. Resistance vs temperature plot for evaporated $Cu_{2.5}Mo_6S_8$ (No. 39). Solid curve is a least-squares fit from Eq. (4).

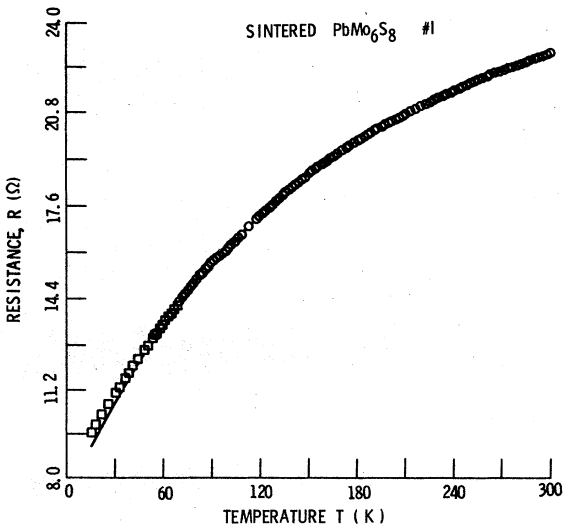

FIG. 6. Resistance vs temperature plot for sintered $PbMo_6S_8$ (No. 1). Solid curve is a least-squares fit from Eq. (4).

comes more important at higher T's.

Parameters in the fits to data for three additional samples are given in Table I (No. 118 $Cu_2Mo_6S_8$, No. 233 $Cu_{2.1}Mo_6S_8$, and sintered $Cu_{1.6}Mo_6S_8$). In all three cases there is a very poor fit to Eq. (3) when $d_n = 0$. When $d_n \neq 0$, reasonably good fits were found using various values of n. That is, plots of Eq. (3) were not too sensitive to the value of n as long as $d_n \neq 0$, and least-squares fits to data were made.

B. "Saturation model" fits

In addition to fits to Eq. (3) we have used data above the inflection point to fit to the "saturation model", represented by Eq. (4). An example of such a fit is shown in Fig. 5 for evaporated $Cu_{2.5}Mo_6S_8$ (No. 39), where data from 30 to 220 K were used. In this and other examples (sintered $PbMo_6S_8$ seen in Fig. 6), the data fit reasonably well in all but the lowest-temperature regions.

Probably the most important result from these plots is the ratio of ρ_{max}/ρ_0, the "resistance ratio". If ρ_{max} is the value of ρ when the electron mean free path is roughly equal to the lattice spacing (as the saturation model assumes),[15,23-27] then the low-temperature (near T_c) mean free path can be estimated from the resistance ratio.[27] Ratios of ρ_{max}/ρ_0 are given in Table I as determined by fits to Eq. (4). Corresponding estimates of the mean free path l at low temperatures are also given, assuming an average lattice spacing of 6.5 Å for the very high-temperature limiting value of l.

C. Magnetoresistance and Hall effect

Figure 7 shows the magnetoresistance of sintered copper to fields of 14 T. This sample exhibited the largest magnetoresistance of the three samples measured. Assuming the materials be-

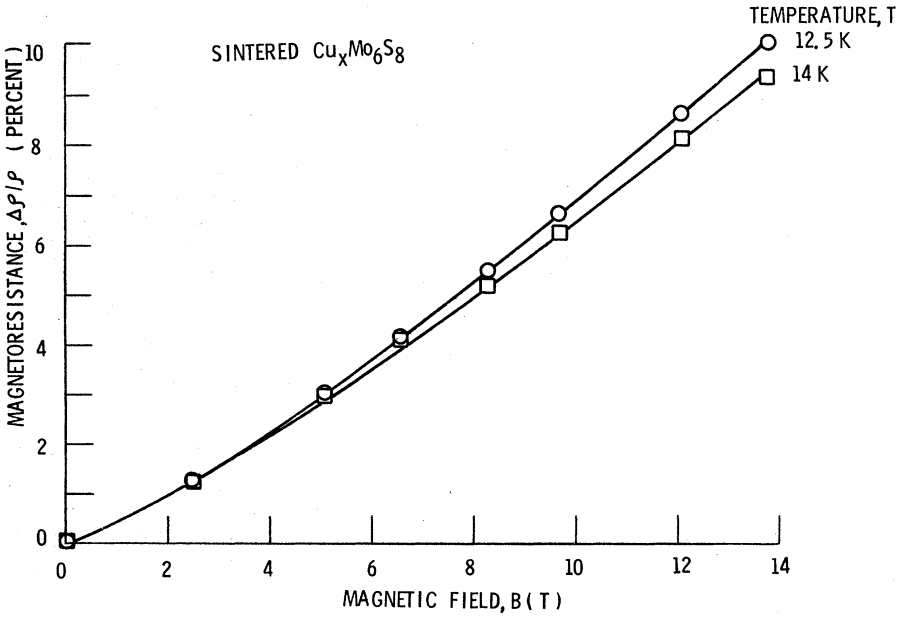

FIG. 7. Magnetoresistance of sintered $Cu_{1.6}Mo_6S_8$ to 14 tesla at 12.5 and 14 K.

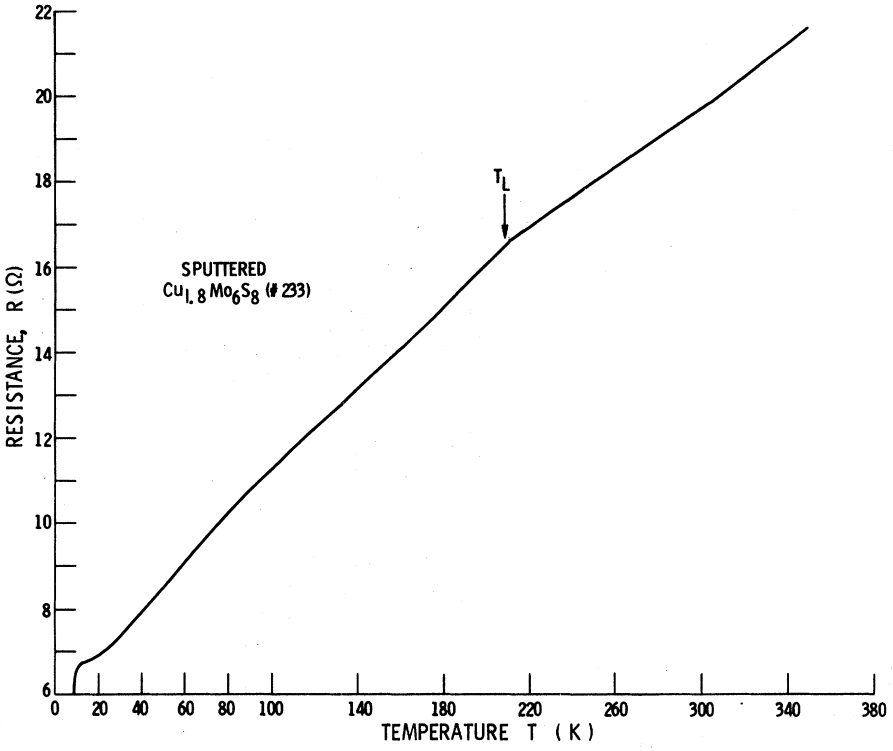

FIG. 8. Resistance vs temperature of sputtered $Cu_{2.1}Mo_6S_8$ (No. 233) showing lattice transformation temperature T_L.

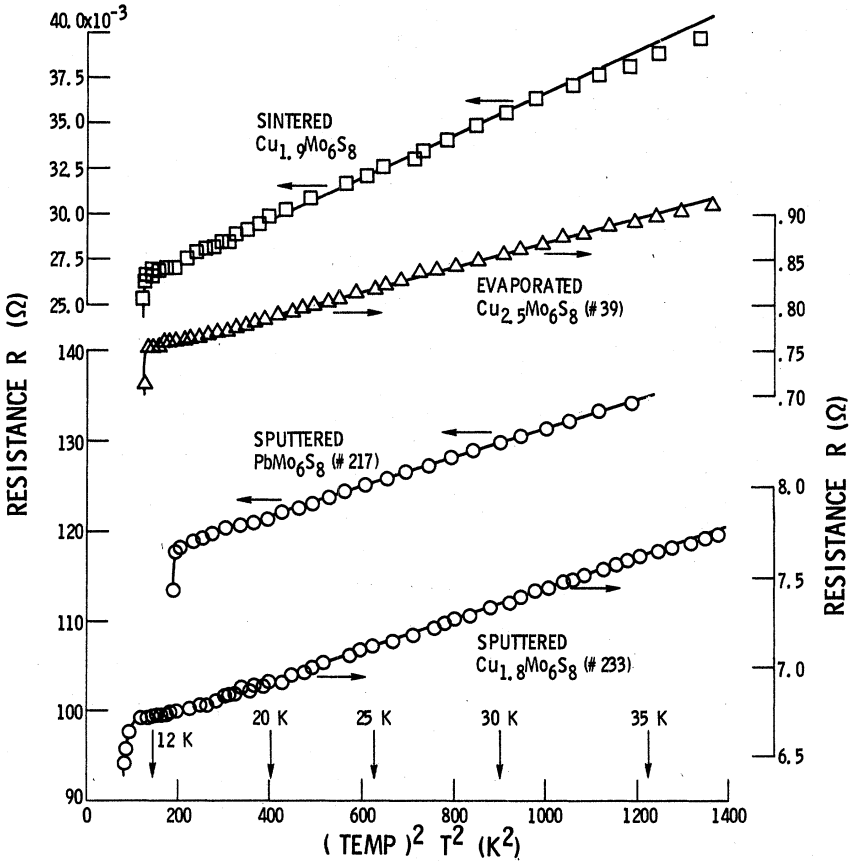

FIG. 9. Resistance vs temperature squared for three $Cu_xMo_6S_8$ and one $PbMo_6S_8$ samples.

TABLE II. Resistance data for various ternary molybdenum sulfides. R_0 and B_0 come from Eq. (2), with $R_0=\rho_0 t/A$ and $B_0=bt/A$, where t is the sample thickness and A the area perpendicular to current flow.

Sample	R_0 (Ω)	B_0 (Ω)	Root-mean-square deviation (%)	No. of points	Range of points (K)	Type behavior
Sputtered $Cu_{2.0}Mo_6S_8$ (No. 118)	1.07	3.23×10^{-4}	0.017	28	11.5–33	T^2
Sputtered $Cu_{2.1}Mo_6S_8$ (No. 233)	6.59	8.39×10^{-4}	0.017	59	12.1–39.4	T^2
Sputtered $Cu_{2.1}Mo_6S_8$ (No. 233)	6.57	8.69×10^{-4}	0.009	43	16.2–35.3	T^2
Evaporated $Cu_{2.5}Mo_6S_8$ (No. 39)	7.32×10^{-2}	1.38×10^{-5}	0.021	32	12.2–31.5	T^2
Sputtered $PbMo_6S_8$ (No. 217)	1.16×10^{2}	1.68×10^{-2}	0.025	15	19.0–31.5	T^2
Sintered $Cu_{1.6}Mo_6S_8$	2.52×10^{1}	1.14×10^{-2}	0.09	25	11.5–31	T^2
Sintered $PbMo_6S_8$ (No. 3)	68.5	7.43×10^{-1}	0.014	27	14.7–41.6	T
Sintered $PbMo_6S_8$ (No. 1)	12.67	1.38×10^{-1}	0.026	21	15.9–42.2	T

TABLE III. Normal-state and superconducting properties of three materials.

	Sputtered $Cu_{2.1}Mo_6S_8$ (No. 233)	Sputtered $PbMo_6S_8$ (No. 217)	Chemical-vapor-deposited Nb_3Sn (Ref. 42)
(ρ_{max}/ρ)	7	3.6	•••
Mean free path l	46 Å	23 Å	160 Å
Hall coefficient R_H	$+2.3\times10^{-24}$ esu	$+0.9\times10^{-24}$ esu	•••
Transition temperature	9.8 K	11.5 K	18.3 K
Critical-field slope $-(dH_{c2}/dT)_{T_c}$	20 kG/K	60 kG/K	18 kG/K
Resistivity ρ_0 (measured)	120 μΩ cm	not measured	10 μΩ cm
Heat-capacity coefficient γ	4000 erg/cm^3 K^2	6400 erg/cm^3 K^2	7300 erg/cm^3 K^2
Resistivity (derived, see text)	65 μΩ cm	125 μΩ cm	•••
Number of carriers, n (holes)	3×10^{22}/cm^3	7×10^{22}/cm^3	9×10^{22}/cm^3
Coherence length ξ_0	86 Å	48 Å	48 Å
Fermi-surface ratio S/S_f	0.44	0.26	0.4
Effective masses m^*/m_0	8	9.6	10.1

TABLE III. *(Continued)*

	Sputtered $Cu_{2.1}Mo_6S_8$ (No. 233)	Sputtered $PbMo_6S_8$ (No. 217)	Chemical-vapor-deposited Nb_3Sn (Ref. 42)
Fermi velocities v_F	6 $\times 10^6$ cm/sec	4 $\times 10^6$ cm/sec	6 $\times 10^6$ cm/sec
Transport relaxation times τ_{tr}	8 $\times 10^{-14}$ sec	5.8×10^{-14} sec	2.5×10^{-13} sec
London-penetration depth, λ_L	2200 Å $\times 10^{-8}$ cm	2400 $\times 10^{-8}$ cm	1400 $\times 10^{-8}$ cm
Ginzburg-Landau constant $K_1(0)$	56	120	34
Thermodynamic critical field $H_c(0)$	1500 G	2230 G	3800 G
Density of states $N(E)$	3.2 $\times 10^{34}$	5.1×10^{34}	5.8×10^{34} erg/cm^3

have like a single-band metal, we determined an average mobility from

$$\mu \simeq (\Delta\rho/\rho)^{1/2} B^{-1}, \tag{5}$$

where μ is in m^2/V sec, and B is in T. Values of μ determined in this way are shown in Table I. The sintered copper had a mobility five to ten times higher than sputtered $PbMo_6S_8$ (No. 217) and sintered $PbMo_6S_8$ (No. 1).

Hall data are shown in Table I, from measurements to 7 T. Between 78 and 60 K there was no change in Hall coefficient within error limits. Assuming a single-band system and

$$R_H = (nec)^{-1}, \tag{6}$$

where n is the carrier concentration and e and c are constants, we get the values of n listed in Table I. All samples had a positive Hall coefficient indicating hole-type carriers. For reasons of sample and lead placement geometry, our values of n are upper limits.

D. Structure in the $Cu_xMo_6S_8$ resistivity versus T data

In Fig. 2 we showed the equilibrium phase diagram as determined by Flükiger *et al.* In the same figure we have drawn bars indicating the position of structure in the ρ vs T data. An example of such structure is shown in Fig. 8 for sputtered $Cu_{2.1}Mo_6S_8$ (No. 233). Similar structure in several electronic properties measurements were used to determine the boundaries in Fig. 2 for samples prepared by melting under argon pressure.[12] The horizontal position for the bars on Fig. 2 were determined by x-ray lattice-constant measurements using the lattice parameter versus x plot shown in Fig. 2 (room-temperature lattice constants). The interesting observation is that of the three samples studied, only No. 118 had a kink at a temperature expected from the phase diagram. Number 233 had a sharp change of slope (Fig. 8), but about 20 K higher than expected. The sintered sample had a broad bump in roughly the expected region, but had a small unexpected jump at about 120 K. Note also the correlation between structure in the a and c values versus x data, and the positions of LT1 and LT2 shown in Fig. 2.

E. Precision low-temperature resistance versus temperature fits

Figure 9 shows $R(T)$ vs T^2 data for sputtered $Cu_xMo_6S_8$, sputtered $PbMo_6S_8$, evaporated $Cu_xMo_6S_8$, and sintered $Cu_xMo_6S_8$. These data were fit using a least-squares method to Eq. (2) (plotting resistance rather than resistivity as explained earlier), and the results are shown in Table II. Resistivities just above T_c were on the order of 100 $\mu\Omega$ cm in sputtered and evaporated samples. (See self-consistent values listed in Table III.) All samples had a T^2 dependence of $R(T)$ over the ranges indicated in Table II, that is, from T_c to nearly 40 K. For the ranges listed in Table II, the root-mean-square deviation of the data from the best fit are given. Figure 9 shows that the data are very good fits to a T^2 dependence.

To ensure reproducibility and physical significance of the data, we measured three different sintered $PbMo_6S_8$ samples made in two independent laboratories. All three sintered samples exhibited a linear dependence of $R(T)$ vs T over the range from T_c to 40 K, and data on two of them are given in Table II. These results were independent of sample and lead geometry and are in direct contrast to the above $R \propto T^2$ results on

all other samples. Fits to Eq. (3) show that the inflection point could be anomalously low for this material. If the first derivative of ρ vs T is slowly changing over the T region just above T_c, ρ could be very nearly linear in T over the extended region given in Table II. Unfortunately, $[dB_{c2}(T)/dT]_{T_c}$ is so large that it would not be practical to measure $\rho(T)$ in a magnetic field (to drive it normal) below the zero field T_c.

IV. CALCULATIONS AND DISCUSSIONS

A. Power law plus exponential fits to $\rho(T)$

Equation (3) was used by Williamson *et al.*[21,22] with $n=1$, $\frac{3}{2}$, or 2. In addition to choosing $n=1$ and $n=2$, we allowed n to become a variable in the least-squares fit to the data to see how the other factors changed, especially T_0. As seen from Table I, we found T_0 to be nearly independent of n for sputtered $PbMo_6S_8$ (No. 217) and evaporated $Cu_{2.5}Mo_6S_8$ (No. 39), but somewhat more dependent on n for all remaining samples. The most "well-behaved" sample was sputtered $PbMo_6S_8$ (No. 217), where data were fit over the widest-temperature region of all samples and fits to the data were very good. The quality of the fits can be seen from the root-mean-square deviations listed in Table I. From Table I note that at 200 K the exponential term in Eq. (3) dominated over the power-law term for sputtered $PbMo_6S_8$ and the terms were somewhat comparable for all other samples. The inflection in $\rho(T)$ vs T occurs at $T_{infl} \simeq \frac{1}{2}T_0$. Fits to Eq. (3) were very poor in all cases where $d_n=0$, i.e., the exponential term significantly improved the fits for all samples. From Table I we see that the values of T_0 are in the range of 50 to somewhat above 100 K for all samples, and this is the region found for similar fits for Nb_3Sn. An exponential term generally occurs in physical phenomena when an energy gap is present and in our case suggests a thermal activation across a gap kT_0.

Williamson *et al.*[21,22] proposed a specific phonon to yield specific values of T_0. The structures of the TMS and the A-15's are very different, as most likely are the Fermi surfaces. The main features these materials have in common are: the Fermi level in a d band with a high density of states at the Fermi energy (see Sec. IV D), a phonon spectrum which softens at lower temperatures, and the presence of lattice instabilities. The similarities of data on the TMS and A-15's presented in the present, as well as later sections is striking.

As a final comment in Sec. IV A we wish to point out that structure in data do not correlate in all cases with the phase diagram derived by Flükiger *et al.* This may be due to a lack of thermodynamic equilibrium in our samples. This conclusion is not without precedent; there are numerous examples of metastable phases in materials.

B. Precision low-temperature fits

Figure 9 and Table II presented details of the excellent fits to Eq. (2) at low temperatures. That is, a T^2 dependence of resistance is found at low temperature for all but the sintered $PbMo_6S_8$ samples. Again, these results are similar to results on A-15 structure materials,[16] where both T^2 (at low temperatures) and fits to Eq. (3) are found.[18-23]

Bader calculated $\rho(T)$ for $PbMo_6S_8$ at low temperature using the phonon spectrum of a sintered sample[36] and obtained a T^2 dependence below 40 K. This result is similar to resistivity data on A-15 materials, explained theoretically by Bader and Fradin[23] on the basis of the associated phonon spectrum. Our results on sintered $PbMo_6S_8$ showing $\rho \propto T$ at low T are in contradiction to these results, in spite of the fact that sputtered $PbMo_6S_8$ and all $Cu_xMo_6S_8$ samples exhibited a T^2 dependence.

Flükiger[11] has measured $R(T)$ in single crystals (believed to be stoichiometric) of various ternary molybdenum sulfides, and finds $R(T) \propto T$ at low temperatures for lead molybdenum sulfide having no Mo_2S_3 present. When Mo_2S_3 is present, a higher than linear power of T is found for $R(T)$, which Flükiger attributes to shorting due to the lower resistivity (by a factor of about 2) of Mo_2S_3 incorporated into his samples. If this were the explanation for our $R \propto T^2$ results, then we would not expect the T^2 behavior over such a wide temperature range (with low root-mean-square deviations—see Table II) as shown in Fig. 9 for the large number of samples studied. The sintered $PbMo_6S_8$ samples were from entirely independent sources and we find no evidence for the presence of Mo_2S_3 in any of our samples, as determined from x-rays.

C. Saturation model fits and mobility

Equation (4) was introduced simply as an empirical fit to the tendency of $\rho(T)$ towards saturation at high T for the A-15 superconductors. We find that it applies quite well for the TMS's. Table I shows the mean free paths derived assuming $\rho \propto l^{-1}$ and $l \simeq 6.5$ Å at high temperatures. This value for high-temperature mean free path is only a rough estimate and could be off by 50% or more. Thus low-temperature mean free paths listed in Table I are only accurate to within 50%.

(All values would be shifted by constant factors if a value different from 6.5 Å were chosen.)

Table I also lists the mean mobility $\bar{\mu}$ as determined from magnetoresistance measurements and with the use of Eq. (5). Note that the sintered $Cu_{1.6}Mo_6S_8$ had a high l, estimated using Eq. (4). This correlates with the relatively high value of $\bar{\mu}$ determined from experiment and Eq. (5), i.e., the sample with the highest mobility had the largest mean free path. Among the other samples mean free paths were comparable to each other, as were mobility values. Grain size was determined by electron microscopy [SEM (scanning-electron microscopy) and TEM (transmission-electron microscopy)], and no correlation of grain size with mean free path or mobility was found. We earlier determined that excess elemental Mo was the flux pinning center determining the superconducting critical current.[37] Scattering centers for limiting mean free paths (and determining $\bar{\mu}$), as well as pinning centers for critical current, are often of comparable (small) size. We thus speculate that excess Mo is the source of both flux pinning and electron scattering. Thus mean free paths and $\bar{\mu}$ are limited by excess Mo.

D. Calculation of normal-state and superconducting parameters

The upper portion of Table III lists the values of a number of measured quantities for three samples: the Hall coefficient R_H, the superconducting transition temperature T_c, the slope of the critical field versus T, $(dH_{c2}/dT)_{T_c}$, a rough estimate of the residual electrical resistivity ρ_0 (a more realistic value of ρ_0 was determined as described below), and the electronic component of the heat capacity γ. Table III also lists values of normal-state and superconducting parameters calculated from standard equations for real metals, as tabulated by Hake.[38] The following relations were used to give the values listed in the lower part of Table III:

$$l = 1.27\times 10^4[\rho n^{2/3}(S/S_f)]^{-1}, \tag{7}$$

where l is the mean free path in cm and S/S_f is the ratio of actual to free-electron Fermi-surface area. Units of ρ are ohm cm and n is in cm^{-3}. The BCS coherence length ξ_0 in cm is given by

$$\xi_0 = 7.93\times 10^{-17} n^{2/3}(S/S_f)(\gamma T_c)^{-1}, \tag{8}$$

where γ is the heat-capacity coefficient in ergs/cm^3K^2 and the Fermi velocity in cm/sec is

$$v_F = 5.76\times 10^{-5} n^{2/3}(S/S_f)\gamma^{-1}. \tag{9}$$

The effective-mass ratio is

$$m^*/m_0 = 6.21\times 10^4 \gamma n^{-1/3}, \tag{10}$$

where m_0 is the rest mass of the electron. The transport scattering time in sec is

$$\tau_{tr} = 2.21\times 10^8 \gamma[\rho n^{4/3}(S/S_f)^2]^{-1}. \tag{11}$$

The density of states (one spin direction) is

$$N(E) = 8\times 10^{30}\gamma(\text{erg cm}^3)^{-1}. \tag{12}$$

The London-penetration depth in cm is

$$\lambda_L = 1.33\times 10^8 \gamma^{1/2}[n^{2/3}(S/S_f)]^{-1}. \tag{13}$$

The Ginzburg-Landau constant

$$K_1(0) \simeq 0.96\lambda_L(1/\xi_0 + 0.7/l) \tag{14}$$

and the thermodynamic critical field $H_c(0)$ in g from BCS theory is

$$H_c(0) = 2.42\,\gamma^{1/2}T_c. \tag{15}$$

Finally,[39]

$$\rho_0 = 2.16\times 10^{-5}(dH_{c2}/dT)_{T_c}[\gamma(1+1.3l/\xi_0)]^{-1}. \tag{16}$$

The quantities ξ_0, v_F, m^*, τ_{tr}, and $N(E)$ are "dressed" since γ is a measured quantity in our equations.

To make the calculations, we took l from fits to Eq. (4) (Table I), $(dH_{c2}/dT)_{T_c}$ from experiment, and n from Eq. (6), then Eqs. (7), (8), and (16) gave values for ρ_0, ξ_0, and S/S_f. The resistivity values derived this way (values listed in lower part of Table III) were probably more reliable than the directly measured value (listed in upper part of Table III) due to uncertainties in thickness measurements. Coherence length to mean-free-path values ξ_0/l were reliable to probably no better than factors of 2 and are model dependent. Both the mobility $\bar{\mu}$ and the density of carriers n were calculated assuming a single band of carriers [Eq. (16)].

Band calculations[40] and other evidence[41] suggest that the Fermi level should lie in a d band originating from Mo d bands. Our results reinforce this interpretation. This is seen in Table III by the high-effective mass and low-Fermi velocity. Nb_3Sn is a d-band metal, and measured and calculated superconducting and normal-state parameters [using Eqs. (7)–(16)] are listed in Table III.[42] The Nb_3Sn data are from a sample prepared by chemical vapor deposition. Table III shows a remarkably linear relation between $N(E)$ and T_c for the three samples. Table III again demonstrates the remarkable similarity between an A-15 material and the TMS.

An important result is that ξ_0 and l are comparable in magnitude. Thus our materials are in the range between clean and dirty superconductors. Sintered samples have a larger $\bar{\mu}$ (see Table I) and thus should be even more in the clean limit. These results are quite significant in that the dirty

limit is often assumed for type II compound superconductors. The data on Nb_3Sn show that l is larger than ξ_0 for the sample listed in Table III.

V. CONCLUSIONS

We have measured the temperature dependence of the resistivity, the magnetoresistance, and the Hall effect on several sputtered, evaporated, and sintered samples of $Cu_xMo_6S_8$. When comboned with superconducting properties measured on the same samples we derive values for the electron mean free path at low temperatures, the Fermi-surface ratio, the density of carriers, the coherence length, the Fermi velocity, the effective mass, the transport scattering time, the London-penetration depth, the Ginzburg-Landau constant, and the thermodynamic critical field. These results indicate that sputtered and evaporated molybdenum sulfides have a low mobility, a large density of carriers are in the range intermediate between clean and dirty superconducting limits, and that the Fermi level probably lies in a high-mass, high-density-of-states d band. Resistivity versus temperature data indicate the applicability of a power law plus exponential expression, where the T_0 in the exponential has values similar to those for A-15 superconductors. A "saturation model" for resistivities at high temperatures is found to apply.

ACKNOWLEDGMENTS

We would like to thank L. Kammerdiner, H. L. Luo, K. C. Chi, R. O. Dillon, R. Bunshah, and S. Bader for supplying samples. We are also indebted to D. C. Martin, E. Haughland, and P. Cataldo for assistance in measurements and computations. One of us (S.A.A.) would like to thank the National Research Council for support as a Senior Research Associate.

---

*Permanent address: Physics Dept., Tel Aviv Univ., Tel Aviv, Israel.

[1]R. Odermatt, ϕ. Fisher, H. Jones, and G. Bongi, J. Phys. C 7, L13 (1974).
[2]S. Foner, E. J. McNiff, and E. J. Alexander, Phys. Lett. A 49, 269 (1976).
[3]S. A. Alterovitz, J. A. Woollam, L. Kammerdiner, and H. L. Luo, Appl. Phys. Lett. 31, 233 (1977).
[4]R. Chevrel, M. Sergent, and J. Prigent, J. Solid State Chem. 3, 515 (1971).
[5]R. Chevrel, Thesis No. 186 (Université de Rennes, 1974) (unpublished).
[6]R. W. McCallum, D. C. Johnston, R. N. Shelton, and M. B. Maple, Solid State Commun. 24, 391 (1977).
[7]B. P. Schweiss, B. Renker, E. Schneider, and W. Reichardt, in *Superconductivity in d- and f-Band Metals*, edited by D. H. Douglass (Plenum, New York, 1977), p. 189.
[8]F. Y. Fradin, G. S. Knapp, S. D. Bader, G. Cinader, and C. W. Kimball, see Ref. 7, p. 297.
[9]S. D. Bader, S. K. Sinha, and R. N. Shelton, see Ref. 7, p. 209.
[10]A. C. Lawson, Mater. Res. Bull 7, 773 (1972).
[11]R. Flükiger, R. Baillif, and E. Walker, Mater. Res. Bull. (to be published).
[12]R. Flükiger, A. Junod, R. Baillif, P. Spitzli, A. Treyvand, A. Paoli, H. Devantay, and J. Muller, Solid State Commun. 23, 699 (1977).
[13]R. A. Hein, in *The Science and Technology of Superconductivity*, edited by Gregory, Mathews, and Edelsack (Plenum, New York, 1973), p. 333.
[14]B. T. Matthias, M. Marezio, E. Corenzeit, A. S. Cooper, and H. E. Barz, Science 175, 1465 (1972).
[15]Z. Fisk and G. W. Webb, Phys. Rev. Lett. 36, 1084 (1976).
[16]G. W. Webb, Z. Fisk, J. J. Engelhardt, and S. D. Bader, Phys. Rev. 15, 2624 (1977).
[17]J. A. Woollam, S. A. Alterovitz, and H. L. Luo, Bull. Am. Phys. Soc. 22, 402 (1977).
[18]D. W. Woodard and G. D. Cody, Phys. Rev. 136, A 166 (1964).
[19]R. W. Cohen, G. D. Cody, and J. J. Halloran, Phys. Rev. Lett. 19, 840 (1967).
[20]V. A. Marchenko, Fiz. Tverd. Tela. (Leningrad) 15, 1893 (1973) [Sov. Phys. Solid State 15, 1261 (1973)].
[21]M. Milewitz, S. J. Williamson, and H. Taub, Phys. Rev. B 13, 5199 (1976).
[22]S. J. Williamson and M. Milewitz, in *Superconductivity in d- and f-Band Metals (1976)*, edited by D. H. Douglass (Plenum, New York, 1977), p. 551.
[23]S. D. Bader and F. V. Fradin, see Ref. 22, p. 567.
[24]P. B. Allen, J. C. K. Hui, W. E. Pickett, C. M. Varma, and Z. Fisk, Solid State Commun. 18, 1157 (1976).
[25]P. B. Allen, Phys. Rev. Lett. 37, 1638 (1976).
[26]M. J. Laubitz, C. R. Leavens, and R. Taylor, Phys. Rev. Lett. 39, 225 (1977).
[27]H. Wiesmann, M. Gurvitch, H. Lutz, A. Gosh, B. Schwarz, and M. Strongin, Phys. Rev. Lett. 38, 782 (1977).
[28]J. A. Woollam, S. A. Alterovitz, and E. Haughland, Phys. Lett. A (to be published).
[29]J. A. Woollam and S. A. Alterovitz, Solid State Commun. 27, 6, 1978.
[30]Kindly provided by Dr. S. D. Bader and Dr. H. L. Luo.
[31]C. K. Banks, L. Kammerdiner, and H. L. Luo, J. Solid State Chem. 15, 271 (1975).
[32]K. C. Chi, R. O. Dillon, R. F. Bunshah, S. A. Alterovitz, and J. A. Woollam, Thin Solid Films 47, L9 (1977).
[33]J. A. Woollam, S. A. Alterovitz, K. C. Chi, R. O. Dillon, and R. F. Bunshah, J. Appl. Phys. 48, 6027 (1978).
[34]K. C. Chi, Thesis (Univer. of Calif., Los Angeles, 1978).
[35]K. C. Chi, R. O. Dillon, R. F. Bunshah, S. A. Alterovitz, and J. A. Woollam, Proceedings of the Third International Conference on Metallurgical Coatings (San Francisco, April 1978) (to be published).
[36]S. D. Bader, Bull. Am. Phys. Soc. 22, 263 (1977);

private communication; Phys. Rev. (to be published).
[37]S. A. Alterovitz, J. A. Woollam, L. Kammerdiner, and H. L. Luo, J. Low Temp. Phys. 30, 797 (1978).
[38]R. R. Hake, Phys. Rev. 158, 356 (1967).
[39]H. Wiesmann, M. Gurvitch, A. K. Gosh, H. Lutz, O. F. Kammerer, and M. Strongin, Phys. Rev. B 17, 122 (1978).
[40]O. K. Anderson, W. Klose, and H. Nohl, Phys. Rev. B 17, 1209 (1978).
[41]ϕ. Fisher, M. Decroux, R. Chevrel, and M. Sergent, in *Superconductivity in d- and f-Band Metals (1976)*, edited by D. H. Douglass (Plenum, New York, 1977), p. 175.
[42]G. D. Cody, H. S. Berman, G. W. Cullen, R. E. Sustrom, J. J. Hanak, R. Hecht, R. L. Novak, and L. J. Vieland, Phenomenon of Superconductivity AFML-TR-65-169, June 1965 (unpublished).